Eidgenössische Technische Hochschule Zürich

Ecole polytechnique fédérale de Zurich
Politecnico federale di Zurigo
Swiss Federal Institute of Technology Zurich

A quadrilateral edge element scheme with minimum dispersion

R. Hiptmair and P.D. Ledger

Research Report No. 2003-17
December 2003

Seminar für Angewandte Mathematik
Eidgenössische Technische Hochschule
CH-8092 Zürich
Switzerland

A quadrilateral edge element scheme with minimum dispersion

R. Hiptmair and P.D. Ledger

Seminar für Angewandte Mathematik
Eidgenössische Technische Hochschule
CH-8092 Zürich
Switzerland

Research Report No. 2003-17 December 2003

Abstract

This paper describes a novel quadrilateral edge element discretisation of Maxwell's equations in which the effects of dispersion are minimised. A modified edge finite element stencil is proposed and it is subsequently shown how this can be expressed in terms of new material coefficients thus allowing us to incorporate both Dirchlet and Neumann boundary conditions in a natural fashion. To demonstrate the success of the proposed procedure, we include a series numerical examples. First we apply the approach to plane and circular wave propagation problems. Secondly, we apply the approach to a series of electromagnetic scattering problems. For the electromagnetic scattering computations, we monitor the effect of the modified edge finite element stencil on the scattering width output. We use a *hp*–edge element code as a benchmark for all our electromagnetic scattering computations.

1 Introduction

The aerospace industry is interested in electromagnetic scattering problems where the wavelength of the wave is short compared to the length of the scatterer. This problems is made more complicated as the scatterer may contain multi–materials and have many sharp corners. In fact, the primary interest lies in the accurate evaluation of the scattering width distribution, which can be computed directly as an output of the scattering problem. This output represents the far field pattern of the scatterer and may be used for the radar detection of civilian and military vehicles.

The $\boldsymbol{H}(\mathrm{curl})$ conforming finite elements first introduced by Nédélec [20, 21, 22] are well suited to such problems as these elements can readily handle material interfaces and boundary conditions. In addition, the spurious modes which are known to occur when components of the field variables are discretised by nodal finite elements do not occur with $\boldsymbol{H}(\mathrm{curl})$ conforming finite elements [23, 19]. Within the engineering community, these elements have become better known as edge elements. This is in part due to the fact that the lowest order $\boldsymbol{H}(\mathrm{curl})$ conforming approximation has a degree of freedom associated with each edge of the element.

When finite element methods are employed to solve wave propagation problems numerical errors often occur. These errors are composed of two parts: Firstly, an error occurs due to interpolation of the continuous solution by discrete functions. Secondly, there is a pollution effect which is due to a phase lag between the computed and exact solution [9]. The pollution effect is often attributed to the difference between the computational and exact wave numbers, also known as the dispersion.

Considerable success at minimising dispersion was obtained when hp–version $\boldsymbol{H}(\mathrm{curl})$ conforming finite elements were used to discretise Maxwell's equations [13, 12]. Indeed, for meshes composed of squares one can directly quantify the dispersion for a given mesh spacing h and polynomial order p [24, 1]. Another interesting approach was proposed in [14] where modified $\boldsymbol{H}(\mathrm{curl})$ conforming finite elements incorporating plane wave expansions were used. However this approach encounted problems when singularities were present in the domain.

In this paper we propose an alternative approach, in which the dispersion is minimised for all wave directions. The idea for this comes from the work of Babuska, Sauter and coworkers [3, 2] who proposed the so called generalised finite element method for Helmholtz equation. In this approach they were able to eliminate the dispersion for one–dimensional problems whilst minimise it for two–dimensional problems. This was achieved by modifying the finite element stencil which results from using standard H^1 conforming 4–noded quadrilaterals for a mesh composed of uniformly sized square elements. Following their approach, we restrict ourselves to two–dimensional problems and modify the finite element stencil for the lowest order quadrilateral edge element on a mesh of uniformly sized squares. We then translate this modification in to a variation in the material coefficients for Maxwell's equations. This allows us to naturally incorporate both Dirchlet and Neumann boundary conditions, something that was not possible with the approach of Babuska and Sauter.

We first apply the scheme to wave propagation problems where we make comparisons with the standard lowest order quadrilateral edge element scheme. Secondly, we apply the standard and modified schemes to electromagnetic scattering problems set in two–dimensions where we use the solutions provided by a hp–edge element code as a reference solution. Electromagnetic scattering problems are set in an infinite domain and in order to make computations possible on a finite computational domain, a perfectly matched layer (PML) [5] is used. We employ this approach due to our previous successes with PML's in the context of hp finite elements [13, 12]. To make an efficient comparison of the electromagnetic scattering solutions we compare the scattering width distributions that are obtained in each case.

The work proceeds as follows: In Section 2 we introduce the variational statement. In Section 3 the quadrilateral edge element discretisation and its accompanying dispersion relationship are given. Then, in Section 4, we propose a modification to quadrilateral edge finite element stencil which allows us to significantly reduce the dispersion. The modified edge finite element stencil is subsequently translated in to new material coefficients allowing the natural incorporation of boundary conditions. Section 5 shows numerical results for a series of wave propagation problems, whilst Section 6 briefly describes the electromagnetic scattering problem and then gives a sequence

of numerical experiments. The paper closes with some concluding remarks.

2 Problem formulation

Let us consider Maxwell's equations expressed in the frequency domain for a source free medium

$$\operatorname{curl} \boldsymbol{E} = -\mathrm{i}\mu\omega \boldsymbol{H} \qquad \operatorname{curl} \boldsymbol{H} = \mathrm{i}\epsilon\omega \boldsymbol{E} \tag{1}$$

where $\boldsymbol{E}$ and $\boldsymbol{H}$ are the electric and magnetic field intensity vectors, ϵ and μ are material parameters, the frequency is such that $\omega^2 > 0$ and $\mathrm{i}^2 = -1$. Initially, we wish to consider domains Ω which are bounded. On the boundary of this domain we apply either Neumann conditions

$$\boldsymbol{n} \wedge \frac{1}{\mu} \operatorname{curl} \boldsymbol{E} = \boldsymbol{n} \wedge \boldsymbol{g} \tag{2}$$

on Γ_{NEU} or Dirchlet conditions

$$\boldsymbol{n} \wedge \boldsymbol{E} = \boldsymbol{n} \wedge \boldsymbol{h} \tag{3}$$

on Γ_{DIR}. Later, when scattering problems are considered, it will be necessary to also include a radiation condition, however, in order to make the presentation more straightforward at this stage this has been omitted.

Combining the Maxwell's curl equations (1) we obtain the vector wave equation for the electric field

$$\operatorname{curl} \frac{1}{\mu} \operatorname{curl} \boldsymbol{E} - \omega^2 \epsilon \boldsymbol{E} = \boldsymbol{0} \tag{4}$$

We note that a similar elimination procedure could also be followed for the magnetic field. However, we wish to focus on the solution of the electric field in this paper and recover, when required, the magnetic field from equation (1). In addition, for the two–dimensional problems in consideration here, we assume that the electric field has components $\boldsymbol{E} = [E_x, E_y]^T$.

With a finite element procedure in mind, we give the weak the variational statement. Find $\boldsymbol{E} \in \boldsymbol{H}_d(\operatorname{curl}; \Omega)$ such that

$$(\mu^{-1} \operatorname{curl} \boldsymbol{E}, \operatorname{curl} \boldsymbol{W})_\Omega - \omega^2 (\epsilon \boldsymbol{E}, \boldsymbol{W})_\Omega = \ell(\boldsymbol{W}) \qquad \forall \boldsymbol{W} \in \boldsymbol{H}_0(\operatorname{curl}; \Omega) \tag{5}$$

where $(\cdot, \cdot)_\Omega$ denotes the standard L^2 inner product performed over Ω and ℓ is a linear form defined as

$$\ell(\boldsymbol{W}) = -\int_{\Gamma_{NEU}} \boldsymbol{W} \cdot \boldsymbol{g} \, \mathrm{d}s \tag{6}$$

The function spaces $\boldsymbol{H}_d(\operatorname{curl}; \Omega)$ and $\boldsymbol{H}_0(\operatorname{curl}; \Omega)$ introduced above are defined as

$$\boldsymbol{H}_d(\operatorname{curl}; \Omega) = \{\boldsymbol{v},\ \boldsymbol{v} \in \boldsymbol{H}(\operatorname{curl}; \Omega)\ \boldsymbol{n} \wedge \boldsymbol{v} = \boldsymbol{n} \wedge \boldsymbol{h},\ \text{on } \Gamma_{DIR}\}$$

$$\boldsymbol{H}_0(\operatorname{curl}; \Omega) = \{\boldsymbol{v},\ \boldsymbol{v} \in \boldsymbol{H}(\operatorname{curl}; \Omega)\ \boldsymbol{n} \wedge \boldsymbol{v} = \boldsymbol{0},\ \text{on } \Gamma_{DIR}\}$$

with

$$\boldsymbol{H}(\operatorname{curl}; \Omega) = \{\boldsymbol{v} \in (L^2(\Omega))^2,\ \operatorname{curl} \boldsymbol{v} \in L^2(\Omega)\}$$

Following a Galerkin finite element procedure, we replace the continuous spaces with discrete subspaces $X_d^H \subset \boldsymbol{H}_d(\operatorname{curl}; \Omega)$ and $X_0^H \subset \boldsymbol{H}_0(\operatorname{curl}; \Omega)$ and solve for discrete solutions $\boldsymbol{E}_H \in X_d^H$. The discrete weak variational statement is then: Find $\boldsymbol{E}_H \in X_d^H$ such that

$$(\mu^{-1} \operatorname{curl} \boldsymbol{E}_H, \operatorname{curl} \boldsymbol{W}_H)_\Omega - \omega^2 (\epsilon \boldsymbol{E}_H, \boldsymbol{W}_H)_\Omega = \ell(\boldsymbol{W}_H) \qquad \forall \boldsymbol{W}_H \in X_0^H \tag{7}$$

In the next section we discuss the discretisation which leads to an approximate solution of this equation.

3 Two–dimensional edge elements on squares

For the purposes of this paper we restrict ourselves to discrete functions based on square elements. These functions are identical to the lowest order quadrilateral edge element basis functions that can be found for example in [1]. Figure 1 shows a square element whose sides are each of length h, the basis functions associated with edges of this element are given as

$$\boldsymbol{\phi}_1 = \begin{matrix} (n+1) - y/h \\ 0 \end{matrix} \qquad \boldsymbol{\phi}_2 = \begin{matrix} y/h - n \\ 0 \end{matrix} \tag{8}$$

$$\boldsymbol{\phi}_3 = \begin{matrix} 0 \\ (m+1) - x/h \end{matrix} \qquad \boldsymbol{\phi}_4 = \begin{matrix} 0 \\ x/h - m \end{matrix} \tag{9}$$

Using these basis functions, an approximation to the electric field inside this element is given by

$$\boldsymbol{E}_H = \sum_{i=1}^{4} \alpha_i \boldsymbol{\phi}_i \tag{10}$$

where the parameters α_1, α_2, α_3 and α_4 represent the degrees of freedom associated with the tangential moments of the field $\boldsymbol{E}_H$ on the element edges.

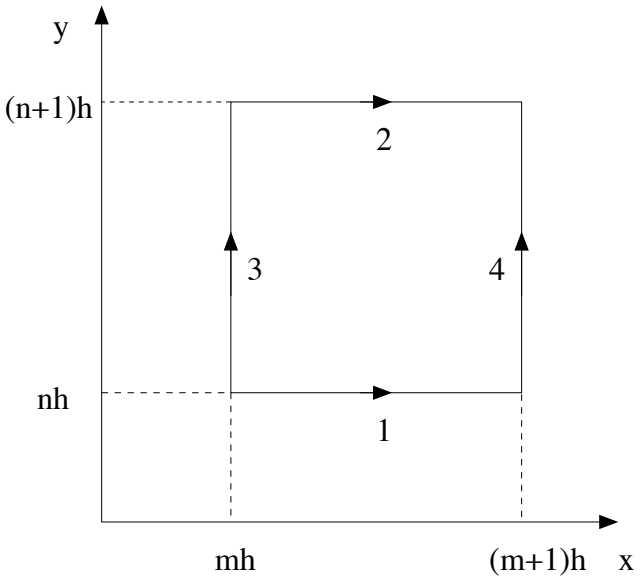

Figure 1: Square edge element with sides of length h.

Let us now assume that the material coefficients of our domain are unit valued and consider the case of elements whose edges do not touch the boundaries of our domain. We wish to form the typical equations which occur in the global stiffness matrix for vertical and horizontal edges. Due to the local support of the basis functions, we are required to consider only elements adjacent to the particular edge in question. Figure 2 shows two typical edges, labelled 1 and 3 and displayed in bold together with their respective neighbouring elements: L and M for the vertical edge and K and M for the horizontal edge. Introducing the notation

$$a(\boldsymbol{E}_H, \boldsymbol{W}_H)_\Omega = (\operatorname{curl} \boldsymbol{E}_H, \operatorname{curl} \boldsymbol{W}_H)_\Omega - \omega^2 (\boldsymbol{E}_H, \boldsymbol{W}_H)_\Omega \tag{11}$$

and then choosing $\boldsymbol{W}_H = \boldsymbol{\phi}_3$ with integration performed over K and L gives

$$\begin{aligned} &a(\boldsymbol{\phi}_3, \boldsymbol{\phi}_3)_{K\cup L}\alpha_3 + a(\boldsymbol{\phi}_8, \boldsymbol{\phi}_3)_L \alpha_8 + a(\boldsymbol{\phi}_9, \boldsymbol{\phi}_3)_L \alpha_9 + a(\boldsymbol{\phi}_{10}, \boldsymbol{\phi}_3)_L \alpha_{10} \\ &\quad + a(\boldsymbol{\phi}_2, \boldsymbol{\phi}_3)_K \alpha_2 + a(\boldsymbol{\phi}_4, \boldsymbol{\phi}_3)_K \alpha_4 + a(\boldsymbol{\phi}_1, \boldsymbol{\phi}_3)_K \alpha_1 = 0 \end{aligned} \tag{12}$$

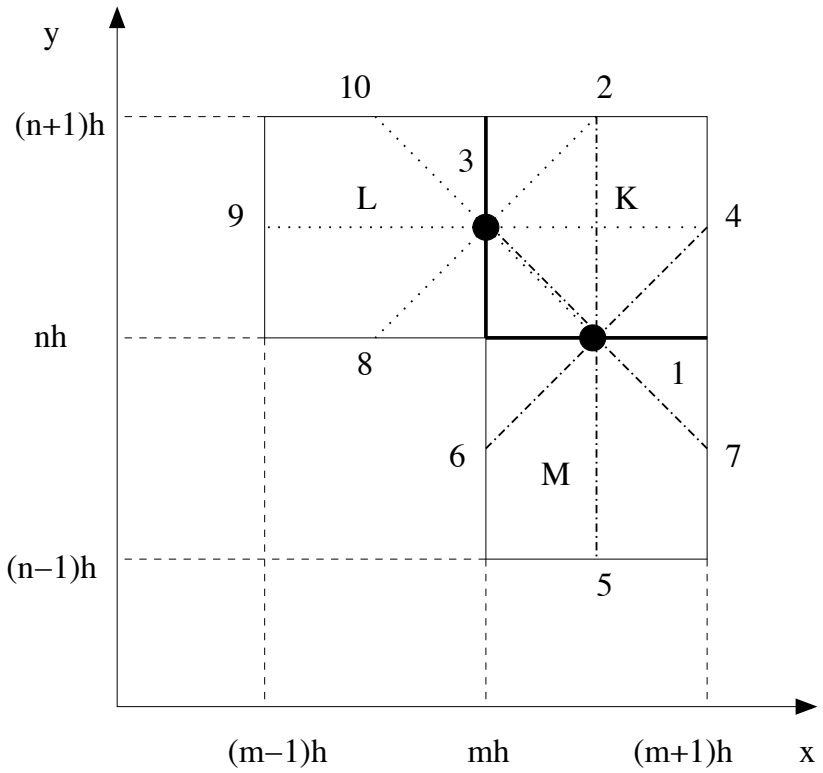

Figure 2: 3 Typical square elements, with edges in consideration for horizontal and vertical stencils shown in bold. The dotted lines show the linkages for a vertical stencil whereas the dashed–dotted lines show the linkages for a horizontal stencil.

where the basis functions for edges $5, 6, 7, 8, 9$ and 10 are given in a similar manner to those presented in equations (8) and (9). The choice of $\boldsymbol{W}_H = \boldsymbol{\phi}_1$ in equation (11) and integration over K and M yields

$$\begin{aligned} &a(\boldsymbol{\phi}_1, \boldsymbol{\phi}_1)_{K\cup M}\alpha_1 + a(\boldsymbol{\phi}_3, \boldsymbol{\phi}_1)_K\alpha_3 + a(\boldsymbol{\phi}_2, \boldsymbol{\phi}_1)_K\alpha_2 + a(\boldsymbol{\phi}_4, \boldsymbol{\phi}_1)_K\alpha_4 \\ &\quad + a(\boldsymbol{\phi}_6, \boldsymbol{\phi}_1)_M\alpha_6 + a(\boldsymbol{\phi}_5, \boldsymbol{\phi}_1)_M\alpha_5 + a(\boldsymbol{\phi}_7, \boldsymbol{\phi}_1)_M\alpha_7 = 0 \end{aligned} \tag{13}$$

¿From equations (12) and (13) one can determine the vertical and horizontal stencils for square edge elements. After performing integration of the various terms, one obtains the following patterns

$$\begin{bmatrix} 2 & & & & & & 3 \\ & -1 & & & 1 & & \\ & & \ddots & \iddots & & & \\ -1 & \cdots & \cdots & 2 & \cdots & \cdots & -1 \\ & & \iddots & \ddots & & & \\ & 1 & & & -1 & & \\ 4 & & & & & & 5 \end{bmatrix} - \omega^2 h \begin{bmatrix} 2 & & & & & & 3 \\ & 0 & & & & 0 & \\ & & \ddots & \iddots & & & \\ \frac{1}{6} & \cdots & \cdots & \frac{2}{3} & \cdots & \cdots & \frac{1}{6} \\ & & \iddots & \ddots & & & \\ & 0 & & & & 0 & \\ 4 & & & & & & 5 \end{bmatrix} \tag{14}$$

for the vertical stencil and

$$\begin{bmatrix} 2 & & -1 & & 3 \\ -1 & & \vdots & & 1 \\ & \ddots & \vdots & \iddots & \\ & & 2 & & \\ & \iddots & \vdots & \ddots & \\ 1 & & \vdots & & -1 \\ & & -1 & & \end{bmatrix} - \omega^2 h \begin{bmatrix} 2 & & \frac{1}{6} & & 3 \\ 0 & & \vdots & & 0 \\ & \ddots & \vdots & \iddots & \\ & & \frac{2}{3} & & \\ & \iddots & \vdots & \ddots & \\ 0 & & \vdots & & 0 \\ & & \frac{1}{6} & & \end{bmatrix} \tag{15}$$

for the horizontal stencil. Furthermore, if one assumes that the discrete solution is the interpolant of the plane wave

$$\boldsymbol{E}_H = \boldsymbol{E}_0 \exp\{\mathrm{i}(\xi_x x + \xi_y y)\} \tag{16}$$

then the solution coefficients can be written in terms of either α_1 or α_3, as follows

$$\begin{array}{ll} \alpha_2 = \alpha_1 \exp\{\mathrm{i}\xi_y h\} & \alpha_4 = \alpha_3 \exp\{\mathrm{i}\xi_x h\} \\ \alpha_5 = \alpha_1 \exp\{-\mathrm{i}\xi_y h\} & \alpha_6 = \alpha_3 \exp\{-\mathrm{i}\xi_x h\} \\ \alpha_8 = \alpha_1 \exp\{-\mathrm{i}\xi_x h\} & \alpha_7 = \alpha_3 \exp\{\mathrm{i}h(\xi_x - \xi_y)\} \\ \alpha_{10} = \alpha_1 \exp\{\mathrm{i}h(\xi_y - \xi_x)\} & \alpha_9 = \alpha_3 \exp\{-\mathrm{i}\xi_x h\} \end{array} \tag{17}$$

Following the approach described by Ainsworth and Coyle [1] we first consider the horizontal edge, then, after inserting the relevant solution coefficients, we obtain the requirement that

$$P\alpha_1 + Q\alpha_3 = 0 \tag{18}$$

In this expression, P and Q take the form

$$P = 2(1 - \cos(h\xi_2) - \frac{\omega^2 h^2}{3}(2 + \cos(h\xi_2)) \tag{19}$$

$$Q = -1 + \exp\{\mathrm{i}\xi_x h\} + \exp\{-\mathrm{i}\xi_y h\} - \exp\{\mathrm{i}h(\xi_x - \xi_y)\} \tag{20}$$

Following a similar procedure for the vertical edge leads to the requirement that

$$Q^*\alpha_1 + R\alpha_3 = 0 \tag{21}$$

where $*$ denotes the complex conjugate and R is given by

$$R = 2(1 - \cos(h\xi_1) - \frac{\omega^2 h^2}{3}(2 + \cos(h\xi_2)) \tag{22}$$

Equations (18) and (21) admit a non–trivial solution α_1, α_3 only if the determinate of the matrix $\begin{matrix} P & Q \\ Q^* & R \end{matrix}$ vanishes. It then follows that that the discrete dispersion relation is given by

$$\omega^2 - \frac{6}{h^2}\frac{1 - \cos(h\xi_x)}{2 + \cos(h\xi_x)} - \frac{6}{h^2}\frac{1 - \cos(h\xi_y)}{2 + \cos(h\xi_y)} = 0 \tag{23}$$

Assuming that $h\xi_x$ and $h\xi_y$ are small the expansion

$$\omega^2 - \quad \xi_x^2 + \xi_y^2 + \frac{1}{12}h^2(\xi_x^4 + \xi_y^4) \quad = O(h^4|\boldsymbol{\xi}|^6) \tag{24}$$

with $\boldsymbol{\xi} = (\xi_x, \xi_y)^T$ may be obtained which allows a quantification of the magnitude of the dispersion.

4 Modified edge finite element stencil

Before describing our modified finite element stencil, we first propose two conditions on our modifications

1. Convergence. We wish that the modified finite element stencil, retains the same structure, sparsity and convergence properties as our original finite element stencil as $h \to 0$;

2. Implementation. We would like to interpret our modified stencil in terms of modified material properties, thereby allowing us to incorporate Dirchlet and Neumann boundary conditions in a natural way.

By restricting ourselves to modified finite element stencils which have the same structure and sparsity of the original finite element stencils, it implies that

$$\begin{array}{ccccccc} & -b & & & & b & \\ & \ddots & & \iddots & & & \\ -b & \cdots & \cdots & e & \cdots & \cdots & -b \\ & \iddots & & \ddots & & & \\ & b & & & & -b & \end{array} - \omega^2 h \begin{array}{ccccccc} & 0 & & & & 0 & \\ & \ddots & & \iddots & & & \\ c & \cdots & \cdots & d & \cdots & \cdots & c \\ & \iddots & & \ddots & & & \\ & 0 & & & & 0 & \end{array} \tag{25}$$

is the form of the vertical stencil and

$$\begin{array}{ccccccc} & & -b & & & & \\ & \ddots & \vdots & \iddots & & & \\ -b & \cdots & e & \cdots & b & & \\ & \iddots & \vdots & \ddots & & & \\ & b & \vdots & & -b & & \end{array} - \omega^2 h \begin{array}{ccccccc} & & c & & & & \\ & \ddots & \vdots & \iddots & & & \\ 0 & \cdots & d & \cdots & 0 & & \\ & \iddots & \vdots & \ddots & & & \\ & 0 & \vdots & & 0 & & \end{array} \tag{26}$$

is the form of the horizontal stencil, where the coefficients b, c, d and e must be chosen.

We wish to interpret the modified edge finite element stencil as new material material parameters. To do this, we evaluate the two–dimensional elemental curl–curl stiffness matrix, $\boldsymbol{S}_{ij}^K = (\mu^{-1}\mathrm{curl}\,\boldsymbol{\phi}_i, \mathrm{curl}\,\boldsymbol{\phi}_j)$ for an element K with constant material coefficient μ

$$\boldsymbol{S}^K = \mu^{-1} \begin{array}{cccc} 1 & -1 & -1 & 1 \\ -1 & 1 & 1 & -1 \\ -1 & 1 & 1 & -1 \\ 1 & -1 & -1 & 1 \end{array} \tag{27}$$

As there is only one free parameter in this matrix, it implies that $\mu^{-1} = b = e/2$ in the stiffness part of the the modified finite element stencils. The ϵ tensor is a 2×2 matrix of the form given below

$$\epsilon = \begin{array}{cc} \epsilon_{11} & \epsilon_{12} \\ \epsilon_{21} & \epsilon_{22} \end{array} \tag{28}$$

We may also evaluate a typical elemental mass matrix $\boldsymbol{M}_{ij}^K = (\epsilon\boldsymbol{\phi}_i, \boldsymbol{\phi}_j)_K$ for an element K with constant material coefficient tensor ϵ as

$$\boldsymbol{M}^K = h^2 \begin{array}{cccc} \frac{\epsilon_{11}}{3} & \frac{\epsilon_{11}}{6} & \frac{\epsilon_{21}}{4} & \frac{\epsilon_{21}}{4} \\ \frac{\epsilon_{11}}{6} & \frac{\epsilon_{11}}{3} & \frac{\epsilon_{21}}{4} & \frac{\epsilon_{21}}{4} \\ \frac{\epsilon_{12}}{4} & \frac{\epsilon_{12}}{4} & \frac{\epsilon_{22}}{3} & \frac{\epsilon_{22}}{6} \\ \frac{\epsilon_{12}}{4} & \frac{\epsilon_{12}}{4} & \frac{\epsilon_{22}}{6} & \frac{\epsilon_{22}}{3} \end{array} \tag{29}$$

By comparing entries in the elemental mass matrix and the mass part of the modified edge finite element stencil, we can make the following observations: In order to retain the structure of the modified edge finite element stencil, the off–diagonal terms of the ϵ tensor should be set to zero. In addition, as the vertical and horizontal stencils have a similar pattern, we recover the fact that $\epsilon_{11} = \epsilon_{22}$. Performing the assembly of elements required for the horizontal and vertical stencils and comparing entries leads to the conclusion that

$$\epsilon = \begin{matrix} 3d/2 & 0 \\ 0 & 3d/2 \end{matrix} = \begin{matrix} 6c & 0 \\ 0 & 6c \end{matrix} \tag{30}$$

Taking all this information in to account, we obtain the following expression

$$\begin{matrix} 2 & & & & & & & 3 \\ 6 & & -b & & & & b & 7 \\ 6 & & \ddots & & \iddots & & & 7 \\ 6 & -b & \cdots & \cdots & 2b & \cdots & \cdots & -b & 7 \\ 6 & & & \iddots & & \ddots & & 7 \\ 4 & & b & & & & -b & 5 \end{matrix} - \omega^2 h \begin{matrix} 2 & & & & & & & 3 \\ 6 & & 0 & & & & 0 & 7 \\ 6 & & \ddots & & \iddots & & & 7 \\ 6 & c & \cdots & \cdots & 4c & \cdots & \cdots & c & 7 \\ 6 & & & \iddots & & \ddots & & 7 \\ 4 & & 0 & & & & 0 & 5 \end{matrix} \tag{31}$$

for the vertical stencil and the expression

$$\begin{matrix} 2 & & & & 3 \\ 6 & & -b & & 7 \\ 6 & -b & \vdots & b & 7 \\ 6 & \ddots & \vdots & \iddots & 7 \\ 6 & & 2b & & 7 \\ 6 & \iddots & \vdots & \ddots & 7 \\ 4 & b & \vdots & -b & 5 \\ & & -b & & \end{matrix} - \omega^2 h \begin{matrix} 2 & & & & 3 \\ 6 & & c & & 7 \\ 6 & 0 & \vdots & 0 & 7 \\ 6 & \ddots & \vdots & \iddots & 7 \\ 6 & & 4c & & 7 \\ 6 & \iddots & \vdots & \ddots & 7 \\ 4 & 0 & \vdots & 0 & 5 \\ & & c & & \end{matrix} \tag{32}$$

for the horizontal stencil. For these stencils, the discrete dispersion expansion becomes

$$\omega^2 - \frac{b}{h^2}\frac{2 - 2\cos(h\xi_x)}{4c + 2c\cos(h\xi_x)} - \frac{b}{h^2}\frac{2 - 2\cos(h\xi_y)}{4c + 2c\cos(h\xi_y)} = 0 \tag{33}$$

which, for the choice of $b = 1$ and $c = 1/6$ one recovers the discrete dispersion relationship for the standard stencil. For small $h\xi_x$ and $h\xi_y$ one can write the expansion

$$\omega^2 - \frac{b}{6c}(\xi_x^2 + \xi_y^2) + \frac{6bc}{12(4c + 2c^2)}(h^2\xi_x^4 + h^2\xi_y^4) = O(h^4|\boldsymbol{\xi}|^6) \tag{34}$$

which allows a quantification of the dispersion for the modified edge finite element stencil. Using this approach, we are now able to incorporate Dirchlet and Neumann boundary conditions in a natural way as modifications to the edge finite element stencil have been translated in to new material coefficients.

4.1 Selection of the coefficients

In order that the modified edge finite element stencil tends to the original edge finite stencil as the mesh spacing $h \to 0$, we choose the coefficients b and c as power series expansions of the following form

$$b = \sum_{i=0}^{N} b_i \omega^{4i} h^{4i} \qquad c = \sum_{i=0}^{N} c_i \omega^{2i} h^{2i} \tag{35}$$

Convergence of the modified edge finite element stencil is then ensured by selecting $b_0 = 1$ and $c_0 = 1/6$ and assuming that ωh is small. A hint as to the correct powers of ωh were provided by

Babuska and Sauter *et. al* [3, 2] who used similar powers in their modified stencil for the Helmholtz equation.

There now exists some degree of freedom in choosing the parameters b_i and c_i for $1 \leq i \leq N$. In the approach of Babuska and Sauter they consider a combined stiffness and mass 9 noded stencil based on a bilinear quadrilateral discretisation of for Helmholtz equation and determine coefficients based on theoretical arguments. Here they attempt to minimise the distance between the exact and stencil behaviour of solutions to the Helmholtz equation. However, by following their approach, it is no longer possible to interpret the modification of the finite element stencil in terms of new material coefficients.

In this work, we adopt a different approach where we choose the coefficients b_i and c_i based on minimising

$$\omega^2 - \frac{b}{h^2}\frac{2-2\cos(h\xi_x)}{4c+2c\cos(h\xi_x)} - \frac{b}{h^2}\frac{2-2\cos(h\xi_y)}{4c+2c\cos(h\xi_y)} \tag{36}$$

assuming that $\xi_x = \omega\cos\phi$ and $\xi_y = \omega\sin\phi$. The procedure we propose is numerical and attempts to minimise this function at a discrete number of wave directions. Further details of the procedure are given below:

Let us assume that a mesh of uniform spacing h has been generated and the true wavenumber of the problem ω has been specified. The strategy we propose is as follows:

1. Set $i = 0$, $b_0 = 1$, $c_0 = 1/6$ and $N = 4$;
2. $i = i + 1$;
3. Let
$$\tilde{b} = \sum_{j=0}^{i} b_j \omega^{4j} h^{4j} \qquad \tilde{c} = \sum_{j=0}^{i} c_j \omega^{4j} h^{4j}$$
where b_i and c_i are unknown coefficients;
4. Determine b_i and c_i such that
$$\max_j \quad \omega^2 - \frac{\tilde{b}}{h^2}\frac{2-2\cos(h\omega\cos\phi_j)}{4\tilde{c}+2\tilde{c}\cos(h\omega\cos\phi_j)} - \frac{\tilde{b}}{h^2}\frac{2-2\cos(h\omega\sin\phi_j)}{4\tilde{c}+2\tilde{c}\cos(h\omega\sin\phi_j)} \quad \to \min$$
where $\phi_j = (2j\pi)/K$ with $j = 1, \cdots, K$, and $K = 20$;
5. If $i \neq N$ goto 2.

There are, of course, many other strategies that could be adopted, including those which attempt to minimise the dispersion over a range of frequencies. But, as the frequency is known for all the examples we consider, it seams logical to adopt a procedure in which the coefficients b_i and c_i are tailored to a given frequency. The procedure presented above is hierarchic in the sense that b_1 and c_1 are first computed, followed by b_2 and c_2 and so forth. It is possible that a better choice of parameters could be obtained if the coefficients b_i, c_i, $i = 1, \cdots, N$ were obtained simultaneously, however this approach may be computationally less advantageous. One could also chose to vary K, the number of angles at which the minimisation procedure is performed and, N the number of terms used in the minimisation procedure. However the choices made above were found to be sufficient for all the computations reported in this work. In any case, we are only interested in discretisations which satisfy $\omega h < 1$, as for larger values of ωh, the assumption of ωh being small, required to ensure the convergence properties of our scheme, is violated. For such cases, the results given by the modified edge finite element stencil may be inaccurate.

To give an initial assessment of the improvement in performance that is obtained by using the modified edge finite element stencil, we consider polar plots of the dispersion

$$\omega^2 - \frac{b}{h^2}\frac{2-2\cos(h\xi_x)}{4c+2c\cos(h\xi_x)} - \frac{b}{h^2}\frac{2-2\cos(h\xi_y)}{4c+2c\cos(h\xi_y)}$$

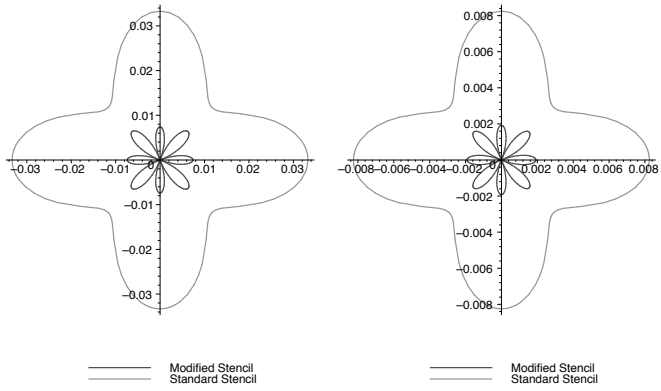

$h = \lambda/10$ $h = \lambda/20$

Figure 3: Polar graphs which compare the dispersive behaviour of the modified and standard edge finite element stencils as a function of angle for the case of $\omega = 1$ and mesh spacings $h = \lambda/10$ and $h = \lambda/20$.

where it is assumed that $\xi_x = \omega \cos\phi$ and $\xi_y = \omega \sin\phi$. Note that in the case of a perfect scheme, the above function would be zero. However neither the original edge finite element stencil or the modified edge finite element stencil are perfect and therefore dispersion is expected in both cases. To quantify the amount of dispersion, we consider the frequency $\omega = 2\pi/\lambda = 1$ and mesh spacings $h = \lambda/10$ and $h = \lambda/20$. Figure 3 shows the results obtained. For both $h = \lambda/10$ and $h = \lambda/20$ we observe that dispersion associated with the modified edge finite element is much smaller than that associated with the standard edge finite element stencil. In the following sections we shall consider numerical examples which show the advantages of using the modified edge finite element stencil in actual finite element computations.

5 Wave propagation problems

We first consider the propagation of the plane wave

$$\boldsymbol{E} = \begin{matrix} k_y \\ -k_x \end{matrix} \quad \exp\{\mathrm{i}(k_x x + k_y y)\} \tag{37}$$

for the case of $k_x = k_y = 5$ on the $(0,1)^2$ square domain. Note that $\omega^2 = k_x^2 + k_y^2$ for this example. Solutions are computed with both Dirchlet and Neumann boundary conditions and on meshes composed of square elements with uniform spacings $h = 1/10, 1/12, 1/14, 1/16, 1/18, 1/20$. The field $\mathrm{Re}(E_x)$ which results from using the standard and modified edge finite elements stencils is then compared with the known exact solution along a diagonal axis through the domain.

Let us consider the case of Dirchlet boundary conditions. These are easily accomplished by setting the coefficients which represent the tangential components of the electric field on the boundary to known values. The results obtained for the sequence of meshes described previously are shown in Figure 4. In this figure, we observe that the dispersion is dramatically reduced when the modified edge finite element stencil is employed, so that on spacings as coarse as $h = 1/10$ which represent approximately 8 points per wave length, the wave is well represented. Using the standard edge finite element stencil, one observes that the dispersion is large even when a mesh with spacing $h = 1/20$ is used. Incidently, this represents a spacing with approximately 18 points per wavelength. We also observe that in the range $h = 1/10$ to $h = 1/20$ the standard edge finite element stencil is in the pre–asymmtopic region where we observe both increases and decreases in the error as the spacing is refined.

Now let us consider the same problem but now solved with Neumann boundary conditions. These boundary conditions are accomplished by discretising equation (6). The results of this

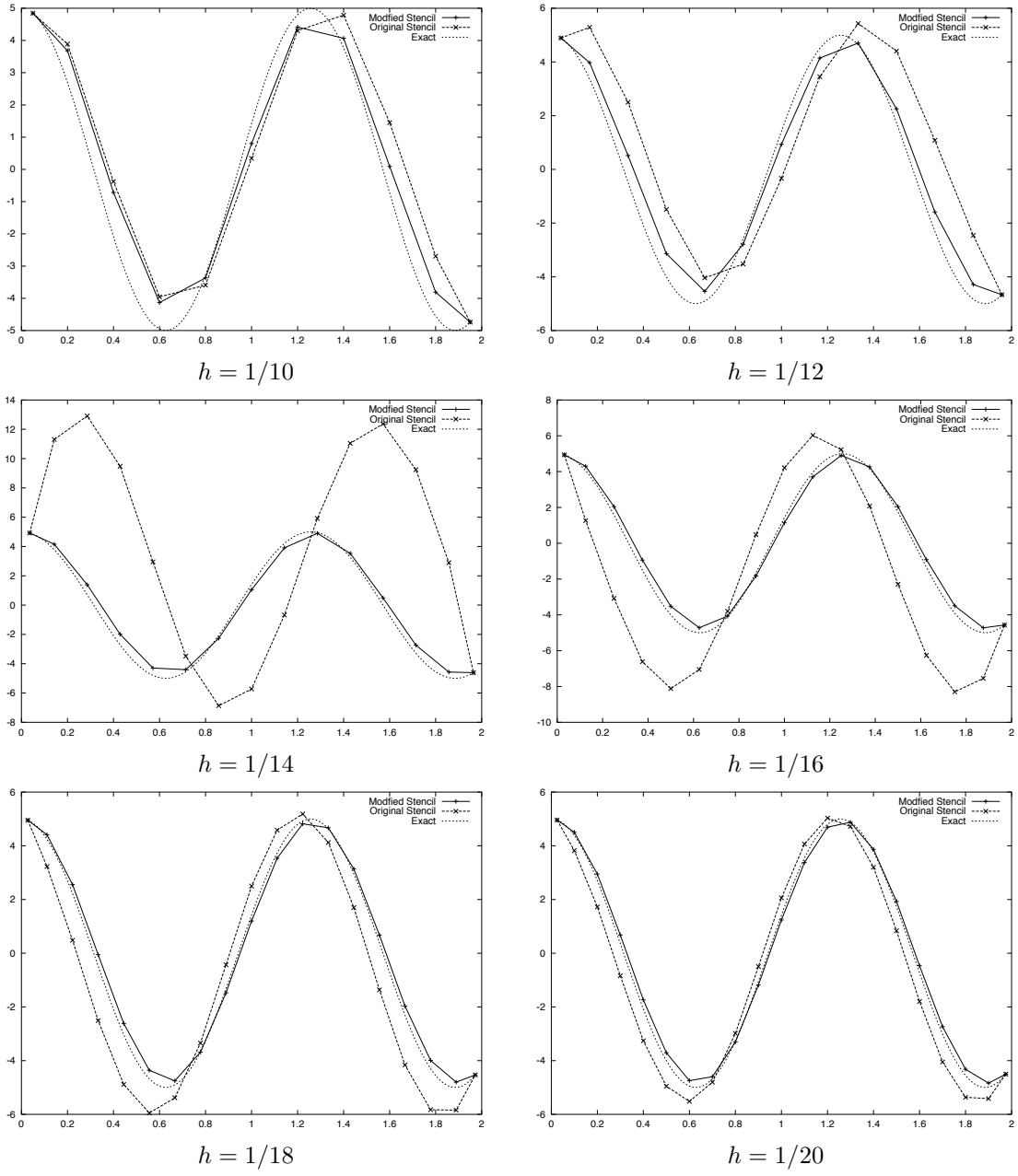

Figure 4: Comparison of the dispersive behaviour of the modified and standard edge finite element stencils for the propagation of a wave with wavenumbers $k_x = k_y = 5$ on a sequence of meshes with different spacings when Dirchlet boundary conditions are employed.

investigation are shown in Figure 5. In this figure, we observe a similar behaviour to what has already been obtained for the case of Dirchlet boundary conditions. The modified edge finite element stencil has a low phase error at coarse mesh spacings whilst the standard edge finite element stencil remains dispersive.

Secondly we consider the propagation of a circular wave, in the form of a Bessel function J_α of order α. The wave we consider is specified as follows

$$\boldsymbol{E} = \begin{matrix} \frac{\partial h}{\partial y} \\ -\frac{\partial h}{\partial x} \end{matrix} \qquad h = J_\alpha(\omega r)\cos\alpha\theta \tag{38}$$

where (r, θ) denote the cylindrical coordinates. We again consider the $(0,1)^2$ square domain and monitor the accuracy of the solution, by computing the $\boldsymbol{H}(\mathrm{curl})$ norm of the error

$$\|\boldsymbol{e}\| = \|\boldsymbol{E}_H - \boldsymbol{E}\| = \int_\Omega |\boldsymbol{e}|^2 + |\mathrm{curl}\,\boldsymbol{e}|^2 \,\mathrm{d}\Omega \tag{39}$$

A sequence of meshes of square elements with uniform spacings $h = 1/9, 1/8, 1/7, 1/6, 1/5, 1/4, 1/3, 1/2$ are considered. We show results obtained with applying Neumann boundary conditions, although similar results can also be obtained by using Dirchlet conditions. Figure 6 shows the convergence of $\|\boldsymbol{e}\|$ obtained for the cases of $\omega = 5$ and $\alpha = 0$, and $\omega = 5$ and $\alpha = 2/3$. The first case represents an example with a smoothly varying field whilst the latter case represents an example case with a singularity at the origin $(0, 0)$. For the case of the smoothly varying field we observe that for coarse mesh spacings the error obtained for the modified edge finite element stencil is worse than than that for the standard stencil. However, when these spacings are considered with respect to the wavelength we observe that they are much coarser than those considered for the plane wave propagation example. In fact, the spacings for which the modified stencil gives worse results represent approximately 6 points per wavelength or coarser. For such spacings the assumption of $\omega h < 1$ is no longer valid and hence an improvement in the error can not be expected. For smaller mesh spacings the error measured in the $\boldsymbol{H}(\mathrm{curl})$ norm is similar to that obtained for standard stencil. A similar convergence behaviour is also observed for the example with a singularity at the origin.

One may of expected that on the basis of the plane wave propagation results, the modified edge finite element stencil should give a substantially lower error than the standard stencil for the propagation of circular waves. However, this extension is not automatic, as the dispersion analysis is carried out for plane waves and not circular waves and hence a reduction in the error for circular waves can not necessarily be expected. Nevertheless, we shall consider the modified stencil for electromagnetic problems which include both behaviour which is similar to both plane and circular waves.

6 Electromagnetic scattering problems

An interesting engineering application of the quadrilateral edge element with minimum dispersion is the electromagnetic scattering problem. Here, the interest lies in the accurate evaluation of the scattering width output which represents the far field pattern of the scattered field. It is hoped that if the dispersion is sufficiently well resolved then the resulting scattering width distribution will be accurately predicted. However, it is expected that for problems with strong singularities, further refinement of the mesh will be needed to accurately resolve the scattering width.

Following the approach described in [13, 12] it is convenient to split the electric field in to incident and scattered fields as

$$\boldsymbol{E} = \boldsymbol{E}^i + \boldsymbol{E}^s \tag{40}$$

where $\boldsymbol{E}^i$ is a known plane wave which satisfies Maxwell's equations and $\boldsymbol{E}^s$ is the scattered field. By linearity, the unknown scattered field also satisfies Maxwell's equations, and this is what should be determined. The scatterer is assumed to be either a perfect electrical conductor (PEC) or a

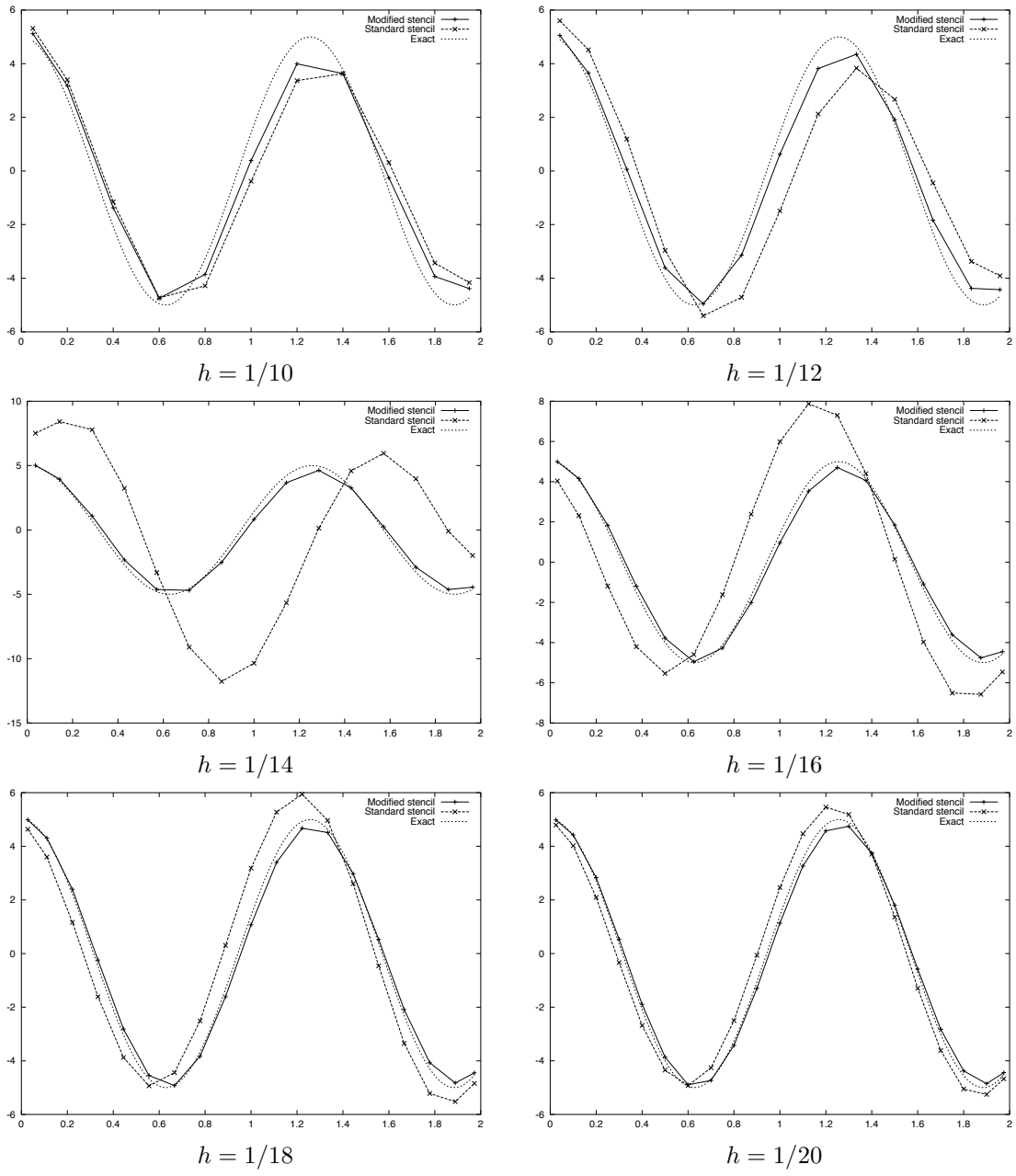

Figure 5: Comparison of the dispersive behaviour of the modified and standard edge finite element stencils for the propagation of a wave with wavenumbers $k_x = k_y = 5$ on a sequence of meshes with different spacings when Neumann boundary conditions are employed.

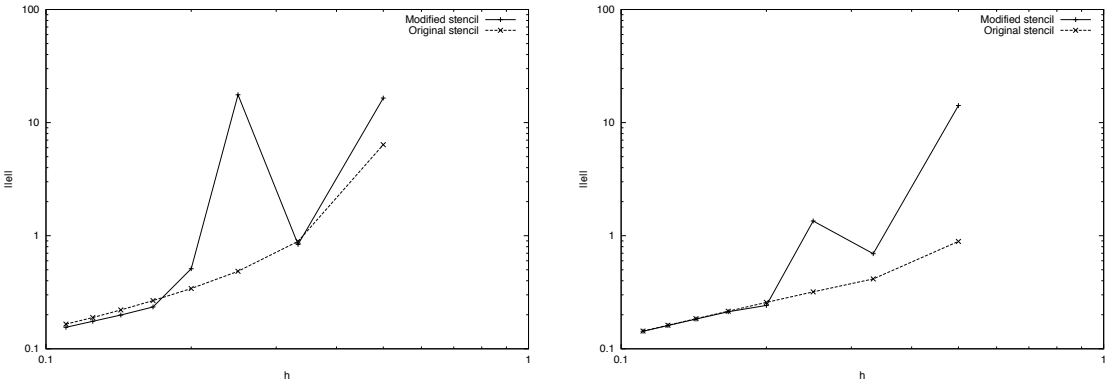

$\alpha = 0$ $\alpha = 2/3$

Figure 6: Comparison of the dispersive behaviour of the modified and standard edge finite element stencils for the propagation of a circular wave with $\omega = 4$ and $\alpha = 0, 2/3$ on a sequence of meshes with different spacings when Neumann boundary conditions are employed.

perfect magnetic conductor (PMC). Although the method we propose is directly extendible to the case where the scatterer contains multi-materials. In the case of a PEC the boundary condition

$$\boldsymbol{n} \wedge \boldsymbol{E}^s = \boldsymbol{n} \wedge \boldsymbol{E}^i \tag{41}$$

is applied on the boundary of the scatterer, Γ_{SCAT}, whilst in the case of a PMC the condition

$$\boldsymbol{n} \wedge \operatorname{curl} \boldsymbol{E}^s = \boldsymbol{n} \wedge \operatorname{curl} \boldsymbol{E}^i \tag{42}$$

is imposed on Γ_{SCAT}.

As mentioned briefly in the introduction, this problem is set in an infinite domain and in order to produce a finite domain for our solution procedure a method of truncation is required. There exist a number of alternatives for accomplishing this, these include absorbing boundary conditions [4], infinite elements [6, 7], the Dirchlet to Neumann map [10], coupling with boundary elements [11] and the use of a perfectly matched layer (PML) [5] The merits of these various approaches are discussed in [13]. For this work we choose to adopt the PML approach due to ease of implementation and previous successes with this approach. As our formulation is based on square elements, it is natural that we choose a rectangular PML. Figure 7 shows a diagram of the scattering problem.

Within the PML layer, modified material parameters are employed to absorb the outgoing scattered wave with minimum reflection. Specifically, we employ

$$\mu = d_1 d_2 \qquad \epsilon = \begin{matrix} \frac{d_2}{d_1} & 0 \\ 0 & \frac{d_1}{d_2} \end{matrix} \tag{43}$$

in Ω_{PML} where $d_j = 1 - \mathrm{i}\sigma_j(x_j)/\omega$ [17]. We adopt a quadratic profile for the grading of σ_j so that $\sigma_j = \sigma(e_j/t)^2$ where e_j is the distance measured from the PML/ free space interface to a point within the PML in a given coordinate direction x_j and t is the PML thickness. Cohen [8] proposes a good choice for t and σ, he selects $t = 1\lambda$ and $\sigma = 6$ and we adopt these values for the computations presented here.

The variational statement for the electromagnetic scattering problem then follows along similar lines to that presented in Section 2. Further details for the interested reader can be found in [13, 12]. We discretise the resulting variational statement using the standard and modified edge finite element stencils and obtain $\boldsymbol{E}^s_H$. Following the finite element solution procedure, one can then proceed to determine scattering width output given by

$$\chi(\phi) = \frac{\omega}{4} \left| \int_{\Gamma_c} \boldsymbol{n} \wedge \boldsymbol{E}^s_H \cdot \boldsymbol{V} + \boldsymbol{n} \wedge \operatorname{curl} \boldsymbol{E}^s_H \cdot \boldsymbol{Y} \, \mathrm{d}\Gamma' \right|^2 \tag{44}$$

where Γ_c is a collection surface which is chosen to completely surround the scatterer and the value of the scattering width measured in Decibels is given by $10\log(\chi(\phi))$. The vectors $\boldsymbol{V}$ and $\boldsymbol{Y}$ are functions of the viewing angle ϕ and are defined as

$$\boldsymbol{V} = \begin{matrix} 0 \\ 0 \\ -1 \end{matrix} \quad \exp\{\mathrm{i}\omega(x'\cos\phi + y'\sin\phi)\} \qquad \boldsymbol{Y} = \frac{1}{\mathrm{i}\omega} \begin{matrix} \sin\phi \\ -\cos\phi \\ 0 \end{matrix} \quad \exp\{\mathrm{i}\omega(x'\cos\phi + y'\sin\phi)\} \tag{45}$$

It is important that the scattering width is calculated carefully, otherwise it is possible that gains in accuracy made with the modified edge finite element stencil may be lost. To this end, we employ the technique proposed by Monk [18, 16], who suggests using the variational statement to approximate the flux term $\boldsymbol{n} \wedge \operatorname{curl} \boldsymbol{E}_H^s$. Further details of its implementation may be found in [12, 15].

6.1 Numerical examples

In this section we present a series of numerical examples to demonstrate the success of using the quadrilateral edge element with minimum dispersion for electromagnetic scattering problems. First we consider a square scatterer of electrical length 3λ, with both PEC and PMC boundaries. We consider an incident wave which is propagated at 45 degrees to the horizontal axis for these examples. Then, we consider a 4λ U shaped cavity rotated through 90 degrees with PEC and PMC boundaries. For these examples, we consider incident plane waves with normal incidences.

First, let us consider scattering by a 3λ PEC square. We consider a domain consisting of a 2λ thick region of free space, backed by a 1λ thick PML. Meshes with uniform spacing $h = \lambda/7, \lambda/8, \lambda/10, \lambda/13$ were generated to discretise this problem. An example mesh with spacing $h = \lambda/17$ is shown in Figure 8. On this sequence of meshes we compare the scattering width distributions which result from using the modified and standard edge finite element stencils with that of a benchmark solution. For the benchmark solution, we use a *hp* edge element code [13, 12, 15], with computations undertaken with a sufficiently small h and high p so as to resolve the problem accurately. Whilst for the comparison, we compute the error in Decibels as the difference between the benchmark and stencil solutions. The results in Figure 9 show that the modified edge finite element stencil is generally more accurate than the standard stencil for the mesh with spacing $h = \lambda/7$. Although, at certain viewing angles, similar errors are obtained for both the modified and standard edge finite element stencils These angles correspond to locations with strong singularities. For finer spacings, the modified edge finite element stencil continues to offer some improvements over the standard stencil. Coarser mesh spacings were not considered, as the assumption $h\omega < 1$ would be violated and for such meshes we expect the solutions using the modified edge finite element stencil to be inaccurate. In Figure 10, a contour plot of $\mathrm{Re}(H_z^s)$ is shown alongside the actual scattering width distribution computed on a mesh with spacing $h = \lambda/13$.

Secondly, we consider scattering by a 3λ PMC square. We employ the same sequence of meshes that were used for the PEC square. The error in the resulting scattering width distributions for the modified and standard edge finite element stencils are shown in Figure 11. In a similar manner to the PEC scatterer, we observe that the modified edge finite element stencil offers some benefits on the coarser meshes. In Figure 12, a contour plot of $\mathrm{Re}(H_z^s)$ is shown alongside the actual scattering width distribution computed on a mesh with spacing $h = \lambda/13$.

Next we consider scattering by a U shape cavity rotated through 90 degrees. The geometry of this cavity is as follows: the thickness of the walls of the cavity are denoted g and the outer dimensions are given by $e + g$ in the x direction and $f + 2g$ in the y direction. The implication is that the inner cavity has dimensions e and f. We consider the particular which is defined by the specific values $e = 4\lambda$, $f = \lambda$ and $g = 0.2\lambda$,. The domain we consider has a 1λ thick region of freespace backed by a 1λ thick PML. We discretise this domain using a sequence of meshes with spacings $h = \lambda/10, \lambda/15, \lambda/20, \lambda/25$. A typical mesh with spacing $h = \lambda/10$ is shown in Figure 13. On each of the meshes we compute the error in the scattering width output for the modified and standard edge finite element stencils when compared with the benchmark solution. The results of these computations can be found in Figure 14. As in the case of the square scatterer we take the

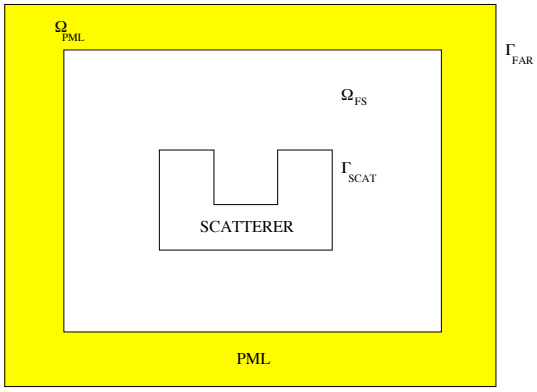

Figure 7: Digram of the electromagnetic scattering problem showing the scatterer, the free space region Ω_{FS} and the PML Ω_{PML}.

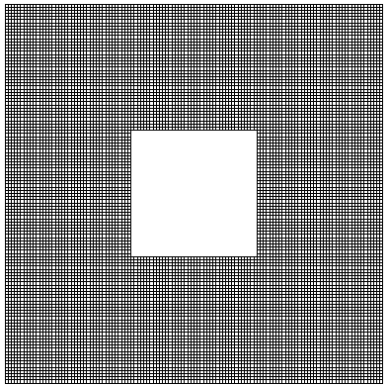

Figure 8: Scattering of plane wave by square of electrical length 3λ showing a mesh of 12800 quadrilateral elements.

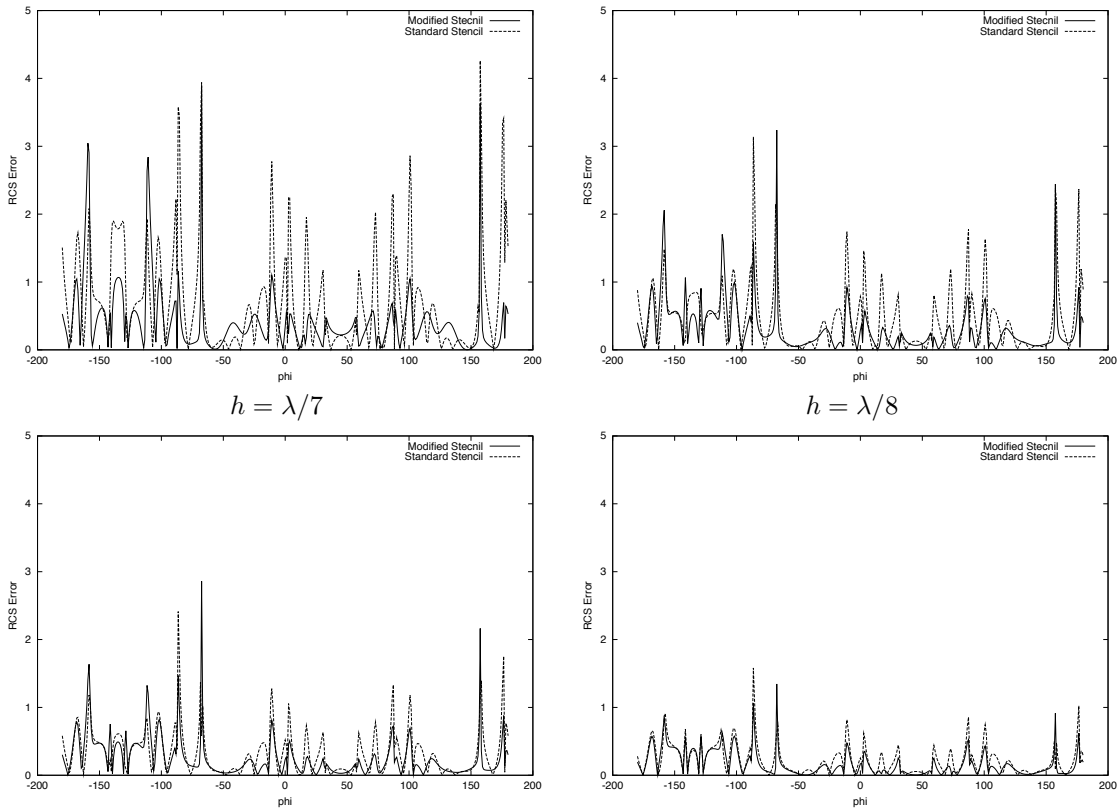

Figure 9: Scattering of plane wave by a PEC square of electrical length 3λ showing the error in the scattering width distributions computed using the modified and standard edge finite element stencils on meshes with spacings $h = \lambda/7, \lambda/8, \lambda/10, \lambda/13$ when compared to the benchmark solution.

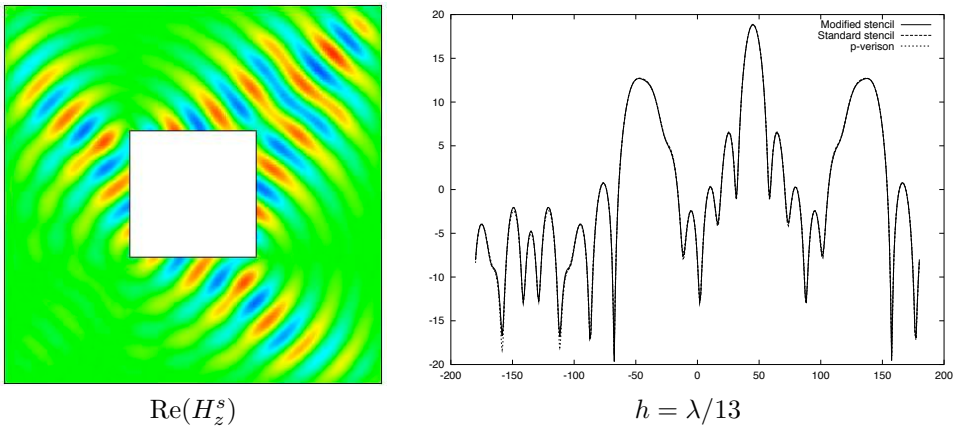

Figure 10: Scattering of plane wave by a PEC square of electrical length 3λ showing a contour plot of $\mathrm{Re}(H_z^s)$ and the scattering width distribution computed on a mesh with spacing $h = \lambda/13$.

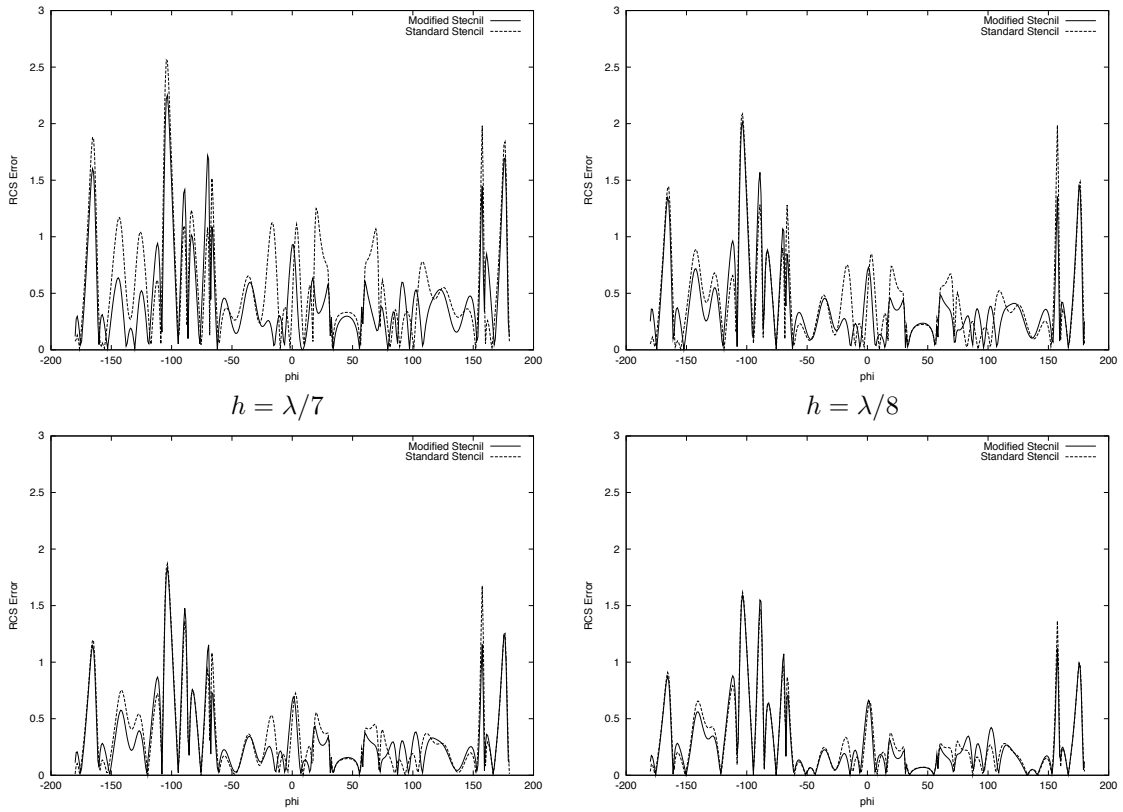

Figure 11: Scattering of plane wave by a PMC square of electrical length 3λ showing the error in the scattering width distributions computed using the modified and standard edge finite element stencils on meshes with spacings $h = \lambda/7, \lambda/8, \lambda/10, \lambda/13$ when compared to the benchmark solution.

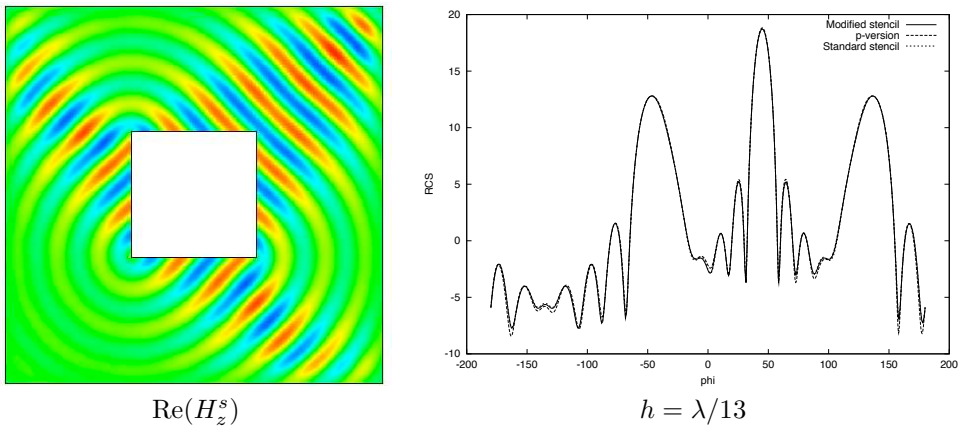

Figure 12: Scattering of plane wave by a PMC square of electrical length 3λ showing a contour plot of $\mathrm{Re}(H_z^s)$ and the scattering width distribution computed on a mesh with spacing $h = \lambda/13$.

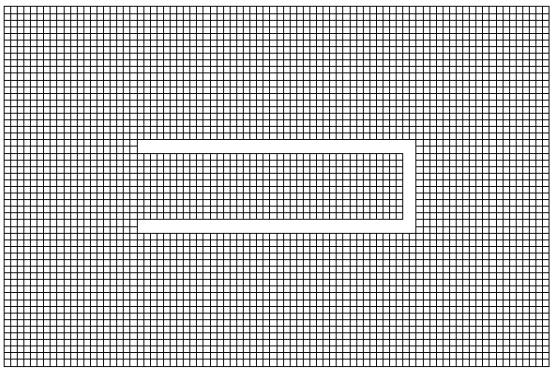

Figure 13: Scattering of plane wave by cavity of electrical length 4λ showing a mesh of 4240 quadrilateral elements.

benchmark solution to be that computed by a *hp* edge element approach with sufficiently fine h and high p. For this scatterer, the modified edge finite element stencil gives a large enhancement over the standard edge finite element stencil. With a mesh as coarse as $h = \lambda/10$ the error in the scattering width obtained with the modified stencil is already much lower than that with the standard stencil. Even for much finer mesh spacings such as $h = \lambda/25$ the standard edge finite element stencil still gives large errors whilst the modified stencil gives accurate results. In Figure 15, a contour plot of $\mathrm{Re}(H_z^s)$ is shown alongside the actual scattering width distribution computed on a mesh with spacing $h = \lambda/25$.

Finally we consider scattering by a 4λ PMC scatterer. For this case, we employ the same sequence of meshes that were used for the PEC scatterer. We compute the error in the scattering width distributions obtained using the modified and standard edge finite element stencils. The results of these computations can be found in Figure 16. In this figure, we observe that on coarsest mesh, with spacing $h = \lambda/10$, the error in the scattering width is much lower with the modified edge finite element stencil compared to the standard stencil, and for meshes with spacings $h = \lambda/15$ or finer a very accurate prediction is obtained. In comparison, we observe that the standard edge finite element stencil remains inaccurate even for the mesh with spacing $h = \lambda/25$. In Figure 17, a contour plot of $\mathrm{Re}(H_z^s)$ is shown alongside the actual scattering width distribution computed on a mesh with spacing $h = \lambda/25$.

Concluding remarks

In the work we have proposed a novel quadrilateral discretisation which allows the magnitude of the dispersion to be substantially reduced. For wave propagation problems it was observed the phase error could be effectively be eliminated for meshes with spacing as coarse as 8 points per wavelength, whereas the standard scheme still remains dispersive at 18 points per wavelength. For circular waves, it was that for $h\omega < 1$, the error measured in the $\boldsymbol{H}(\mathrm{curl};\Omega)$ norm was similar to that for standard scheme.

For scattering problems, with discretisations satisfying $h\omega < 1$ accurate predictions of the scattering width distribution were obtained with the modified stencil. The more complex the scatterer, the clearer the benefits became. This was illustrated by the complex scattering which occurs within a U shape scatterer rotated through 90 degrees. For this example, using the modified edge finite element stencil and a coarse mesh of spacing $h = \lambda/10$ it was found that one can accurately capture the scattering width distribution. Whilst, use of the standard edge finite element stencil required much finer mesh spacings to give an accurate prediction.

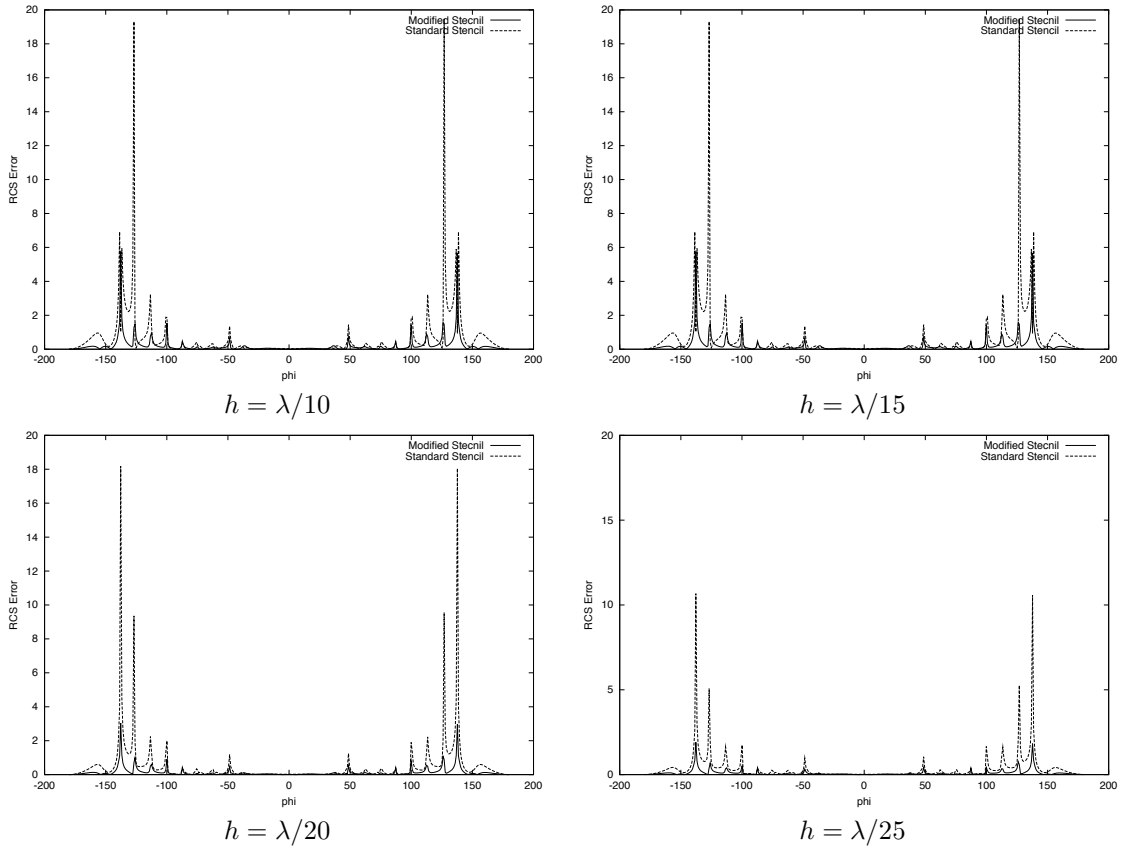

$h = \lambda/10$ $h = \lambda/15$

$h = \lambda/20$ $h = \lambda/25$

Figure 14: Scattering of plane wave by a PEC cavity of electrical length 4λ showing the error in the scattering width distributions computed using the modified and standard edge finite element stencils on meshes with spacings $h = \lambda/10, \lambda/15, \lambda/20, \lambda/25$ when compared with the benchmark solution.

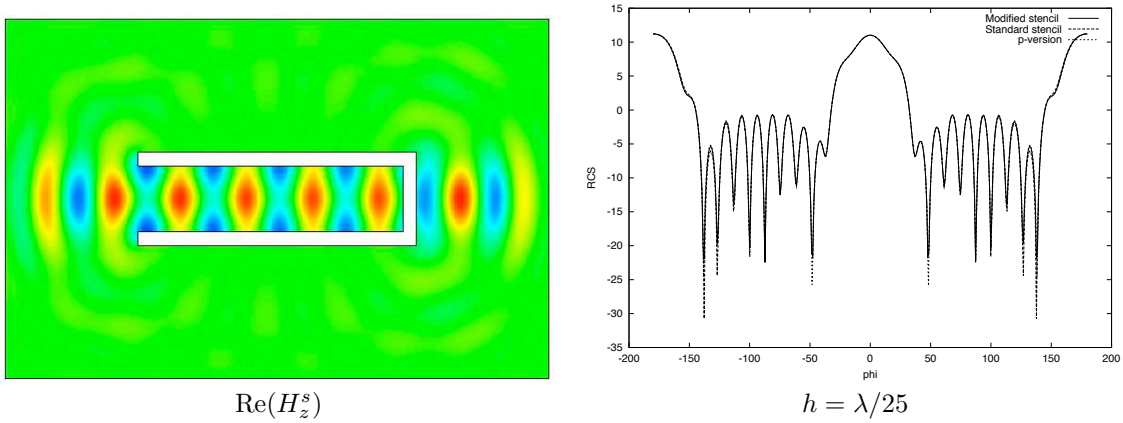

$\mathrm{Re}(H_z^s)$ $h = \lambda/25$

Figure 15: Scattering of plane wave by a PEC cavity of electrical length 4λ showing a contour plot of $\mathrm{Re}(H_z^s)$ and the scattering width distribution computed on a mesh with spacing $h = \lambda/25$.

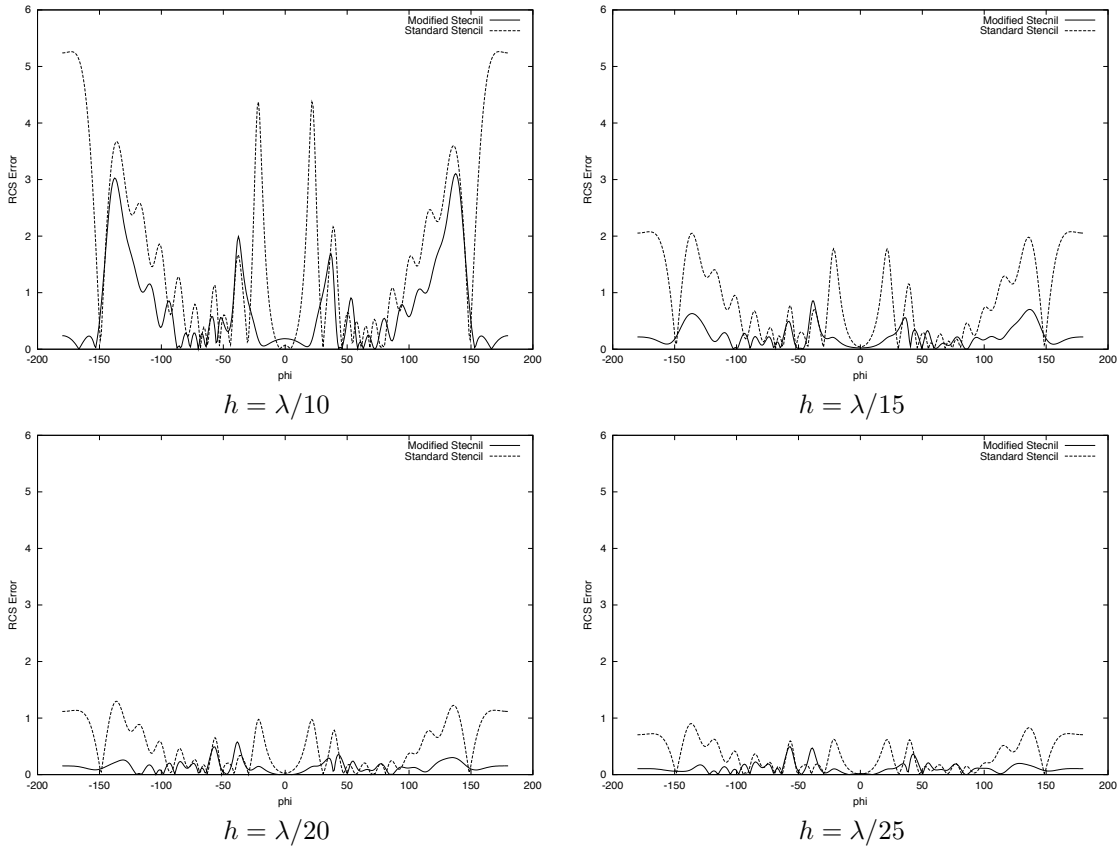

$h = \lambda/10$ $h = \lambda/15$

$h = \lambda/20$ $h = \lambda/25$

Figure 16: Scattering of plane wave by a PMC cavity of electrical length 4λ showing the error in the scattering width distributions computed using the modified and standard edge finite element stencils on meshes with spacings $h = \lambda/10, \lambda/15, \lambda/20, \lambda/25$ when compared with the benchmark solution.

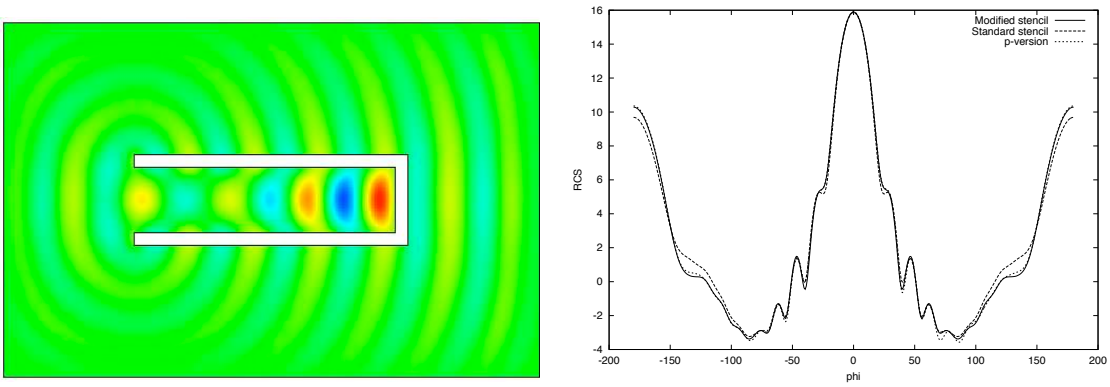

$\mathrm{Re}(H_z^s)$ $h = \lambda/25$

Figure 17: Scattering of plane wave by a PMC cavity of electrical length 4λ showing a contour plot of $\mathrm{Re}(E_z^s)$ and the scattering width distribution computed on a mesh with spacing $h = \lambda/25$.

References

[1] M. Ainsworth and J. Coyle. Hierarchic *hp*–edge element families for Maxwell's equations on hybrid quadrilateral/triangular meshes. *Computer Methods in Applied Mechanics and Engineering*, 190:6709–6733, 2001.

[2] I.M. Babuska, F. Ihlenburg, E.T. Paik, and S.A. Sauter. A generalised finite element method for solving the Helmholtz equation in two dimensions with minimal pollution. *Computer Methods in Applied Mechanis and Engineering*, 128:325–359, 1995.

[3] I.M. Babuska and S.A. Sauter. Is the pollution effecit of the FEM avoidable for the Helmholtz equation considering high wave numbers? *SIAM Review*, 42:451–484, 2000.

[4] A. Bayliss and E. Turkel. Radiation boundary conditions for wave–like equations. *Communications in Pure and Applied Mathematics*, 33:707–725, 1980.

[5] J-P Berenger. A perfectly matched layer for the absorption of electromagnetic waves. *Journal of Computational Physics*, 114:185–200, 1994.

[6] P. Bettess. *Infinite Elements*. Penshaw Press, Sunderland, 1992.

[7] W. Cecot, L. Demkowicz, and W. Rachowicz. A two dimensional infinite element for Maxwell's equations. *Computer Methods in Applied Mechanics and Engineering*, 188:625–643, 2000.

[8] G.C. Cohen. *Higher Order Numerical Methods for Transient Wave Eqautions*. Springer, 2002.

[9] A. Deraemaeker, I. Babuska, and P. Bouillard. Dispersion and pollution of the FEM solution for the Helmholtz equation in one, two and three dimensions. *International Journal for Numerical Methods in Engineering*, 46:471–499, 1999.

[10] D. Givoli. *Numerical Methods for Problems in Infinite Domains*. Elsevier, Amsterdam, 1992.

[11] R. Hiptmair. Coupling of finite elements and boundary elements in electromagnetic scattering. *SIAM Journal of Nuermical Analysis*. accepted.

[12] P.D. Ledger. *An hp-Adaptive Finite Element Proceedure for Electromagnetic Scattering Problems*. PhD thesis, Dept. Civil Engineering, University of Wales, Swansea, 2002.

[13] P.D. Ledger, K. Morgan, O. Hassan, and N.P. Weatherill. Arbitrary order edge elements for electromagnetic scattering simulations using hybrid meshes and a PML. *International Journal for Numerical Methods in Engineering*, 55:339–358, 2002.

[14] P.D. Ledger, K. Morgan, O. Hassan, and N.P. Weatherill. Plane wave $\boldsymbol{H}(\mathrm{curl})$ conforming finite elements for Maxwell's equations. *Computational Mechanics*, 31:272–383, 2003.

[15] P.D. Ledger, J. Peraire, K. Morgan, O. Hassan, and N.P. Weatherill. Efficient highly accurate *hp*-adaptive finite element computations of the scattering width output of Maxwell's equations. *International Journal for Numerical Methods in Fluids*, 43, 2003.

[16] P. Monk. The near to far field transformation. *COMPEL The International Journal for Computation and Mathematics in Electrical and Electronic Engineering*, 14:41–56, 1995.

[17] P. Monk. *Finite Element Method for Maxwell's Equations*. Oxford Science Publications, 2003.

[18] P. Monk and E. Suli. The adaptive computation of far field patterns by a posteriori error estimation of linear functionals. *SIAM Journal of Numerical Analysis*, 36:251–274, 1998.

[19] G. Mur. Edge elements, their advantages and their disadvantages. *IEEE Transactions on Magnetics*, 30:3552–3557, 1994.

[20] J.C. Nédélec. Computation of Eddy currents on a surface in $\mathbb{R}^3$ by finite element methods. *SIAM Journal of Numerical Analysis*, 15:580–594, 1978.

[21] J.C. Nédélec. Mixed elements in $\mathbb{R}^3$. *Numerische Mathematik*, 35:315–341, 1980.

[22] J.C. Nédélec. A new family of mixed elements in $\mathbb{R}^3$. *Numerische Mathematik*, 50:57–81, 1986.

[23] D. Sun, J. Manges, X. Yuan, and Z. Cendes. Spurious modes in finite-element methods. *IEEE Antennas and Propagation Magazine*, 37:12–24, 1995.

[24] G.S. Warren and W.R. Scott. An investigation of the numerical dispersion in the vector finite element method using quadrilateral elements. *IEEE Transactions on Antennas and Propagation*, 42:1502–1508, 1994.

Research Reports

No.	Authors	Title
03-17	R. Hiptmair, P.E. Ledger	A quadrilateral edge element scheme with minimum dispersion
03-16	R. Jeltsch, K. Nipp	Adapting the CSE program at ETH Zurich to the Bologna process
03-15	R. Hiptmair, P.E. Ledger	Computation of Resonant Modes for Axisymmetric Cavities using *hp*-Version Finite Elements
03-14	V.H. Hoang, C. Schwab	High-dimensional finite elements for elliptic problems with multiple scales
03-13	A. Toselli, X. Vasseur	A numerical study on Neumann-Neumann methods for *hp* approximations on geometrically refined boundary layer meshes II: Three-dimensional problems
03-12	X. Feng, M. von Oehsen, A. Prohl	Rate of Convergence of Regularization Procedures and Finite Element Approximations for the Total Variation Flow
03-11	P.-A. Nitsche	Best N Term Approximation Spaces for Sparse Grids
03-10	J.T. Becerra Sagredo	Z-splines: Moment Conserving Cardinal Spline Interpolation of Compact Support for Arbitrarily Spaced Data
03-09	P. Houston, D. Schötzau, Th. Wihler	Energy norm a-posteriori error estimation for mixed discontinuous Galerkin approximations of the Stokes problem
03-08	R. Hiptmair, A. Buffa	Coercive combined field integral equations
03-07	R. Hiptmair, O. Sterz	Current and Voltage Excitations for the Eddy Current Model
03-06	A.-M. Matache, P.-A. Nitsche, C. Schwab	Wavelet Galerkin Pricing of American Options on Lévy Driven Assets
03-05	M. Becheanu, R.A. Todor	On the Set of Diameters of Finite Point-Sets in the Plane
03-04	C. Schwab, R.A. Todor	Sparse finite elements for stochastic elliptic problems - higher order moments
03-03	R. Sperb	Bounds for the first eigenvalue of the elastically supported membrane on convex domains
03-02	F.M. Buchmann	Computing exit times with the Euler scheme
03-01	A. Toselli, X. Vasseur	Domain decomposition preconditioners of Neumann-Neumann type for *hp*-approximations on boundary layer meshes in three dimensions